Calibration of alpha function for density prediction of general fluids

Abstract

An analytical expression of equation of state (EOS) is required for the closure of conservation laws in fluid flow simulations in a computational framework. However, many empirical EOS fail to provide accurate predictions of thermodynamic properties over a broad range of fluid states, such as compressed-liquid, supercritical-fluid, and near-critical states, typical of propellants involved in many propulsion and power-generation systems. In the present work, a modified Peng-Robinson EOS is proposed by calibrating the alpha function in a statistical manner. Semi-parametric alpha functions are developed as the sum of a parametric computer model and a statistical correction accounting for model discrepancy. The latter is necessary to capture the trend of alpha variation under different conditions. The accuracy of semi-parametric alpha functions is examined in detail for the density prediction of representative substances, including oxygen, carbon dioxide, and n-decane. Results show that the semi-parametric alpha function with two variable parameters and three calibration parameters provides consistently superior accuracy of estimation of density over wide ranges of temperature and pressure at all thermodynamic states. The average relative error for the studied substances is below 0.5% at different pressures. The modified PR EOS can be further incorporated into large-scale multiphysics simulations where real-fluid behavior occurs.

*corresponding author (wangx@fit.edu)

Keywords: calibration, Peng-Robinson equation of state, alpha function, supercritical fluid

1. Introduction

An equation of state (EOS) is an analytical expression relating pressure to temperature and volume of a fluid for evaluations of volumetric behaviors, thermodynamic properties, and phase equilibria of fluids and fluid mixtures. Such an expression is required for the closure of conservation equations in multi-physics simulations [1-4]. Since the development of the van der Waals (vdW) EOS, hundreds of empirical modifications have been proposed to improve thermodynamic predictions, and those EOS vary from cubic-type to virial-type to molecular-based equations [5-7]. However, there is currently no single all-in-one EOS that gives the best prediction of all substances at all fluid states. For example, two widely used cubic EOS, Soave-Redlich-Kwong (SRK) [8] and Peng-Robinson (PR) [9], show large errors in estimating density in regions of compressed liquid, near-critical point, and supercritical fluid. These regions are closely related to the states of working fluids in modern power-generation and transportation systems, including supercritical CO_2 power cycles, liquid-rocket engines, and diesel engines. The accuracy of the EOS determines the reliability of predictive tool development in these systems. For example, predictions of thermodynamic properties are directly related to the prediction of flame temperature and emission concentrations in hydrocarbon combustion [10, 11]. To this end, the present work applies an advanced statistical learning technique to develop a robust cubic EOS based on the PR EOS. The new EOS can provide significantly improved accuracy in the thermodynamic regions where the traditional cubic EOS underperform.

The most accurate EOS to date for pure substances is the modified Benedict–Webb–Rubin (mBWR) equation [12], a virial-type equation that includes 32 terms with numerical parameters determined by fitting the equation to empirical data. The mBWR EOS has been incorporated into the popular software package REFPROP, developed by the National Institute of Standards and Technology (NIST) [13]. However, the mBWR EOS suffers from two major disadvantages: (1) the large number of adjustable parameters make it difficult to extend to mixtures, and (2) its analytical complexity results in time-consuming computation, especially when incorporated into multi-scale, multi-physics simulations. In order to avoid the introduction of additional complexity to existing simulations, it is desirable to develop an EOS that has a simple expression as a cubic EOS, like SRK and PR, and is as accurate as mBWR.

Modifications of cubic EOS have revolved around three different approaches [7]: (1) introducing deviation functions (volume translation), (2) adding new parameters, and (3) changing the dependence structure of the alpha function. Volume translation methods introduce a correction term to the molar volume accounting for the deviation of liquid density between experimental data and calculations [14]. The second approach, such as three-parameter [15] and four-parameter [16] EOS, involves the addition of parameters in the attractive or repulsive term, and can capture the correct critical compressibility factor for different fluids but at the cost of increased calculation complexity. Extensive efforts have been put into developing accurate expressions of the alpha function, including the Soave-type alpha functions [8, 9, 17, 18] and exponential alpha functions [19-22]. The first two approaches require a significant change of the EOS expression and thus increase the calculation complexity, while the third approach maintains the simplicity of the functional form of the cubic EOS. The present work focuses on improvements to the alpha function.

Soave-type alpha functions express alpha as a function of reduced temperature with a characteristic constant correlated to the acentric factor of the substances. Twu et al. [22] developed an exponential alpha function that improved the prediction of vapor pressure at low reduced temperature for both light and heavy hydrocarbons. Other exponential alpha functions have been proposed for different substances under different conditions [19-21]. Forero and Velásquez [23] made detailed comparisons among different alpha functions for two-parameter and three-parameter cubic EOS.

As noted by Lopez-Echeverry et al. [7], further development of a universal, simple and accurate EOS is still a rich source for research and discussion, since the success of existing modifications is restricted to the properties studied and the compounds of interest. Additional restrictions include the limited range of experimental data used for training the parameters in the alpha function and the optimization method used to determine these parameters. Almost all existing EOS were trained using data in the liquid-vapor saturation region, together with the phase equilibrium constraint. This is one of the main causes of poor predictions in other regions of the thermodynamic phase diagram, such as the compressed-liquid, near-critical, and supercritical regions. Furthermore, the parameters involved in existing EOS were determined by minimizing an objective function through an iterative procedure. The objective functions that have employed in reported studies include fugacity coefficient difference [8, 9] and relative error of vapor pressure and/or liquid density [19, 20, 24]. The adopted optimization techniques were generally *ad hoc* and could cause overfitting and underfitting issues.

Recent advances in statistical calibration [25-27] can provide new insight into this problem. Recognizing the fact that the true mathematical form of the EOS is unknown, the existing cubic

EOS (for example, SRK and PR) are simple and inexact models that are used to approach the true pressure-volume-temperature relationship. The present work not only calibrates the optimal parameters to minimize the error between the model and reality, but also considers a model bias from inexact models, which represents the difference between the model and physical reality. Calibration is a process of using data from physical experiments to learn and adjust the parameters of inexact computer models. This technique treats the output from physical experiments as a realization of a stochastic process, providing a statistical basis for the determination of parameters [28]. Kennedy and O'Hagan [25] formulated a Bayesian framework to calibrate the parameters of computer models by considering all sources of uncertainties, including parameter uncertainty, model discrepancy, and measurement error. The work has made a large impact in various fields where inexact computer models are used and must be calibrated (See, for example, Refs. [29-33]). Tuo and Wu [26] pointed out theoretically the potential unidentifiability issue of the model parameter in Kennedy and O'Hagan [25] and proposed an L_2 calibration method that shows the semiparametric efficiency . Plumlee [27] showed that the prior distribution of the model bias should be orthogonal to the gradient of the model function and provided an alternative prior for the Bayesian calibration of computer models.

Motivated by the nature of the cubic EOS and the aforementioned restrictions of parameter estimation techniques, semi-parametric alpha functions are proposed using a statistical calibration technique that leverages physical data in all thermodynamic regions and aims to produce optimal and identifiable parameters for the model form of the EOS. The semi-parametric alpha functions consist of a parametrized computer model and a statistical correction accounting for the model discrepancy and measurement error. The accuracy of various semiparametric alpha functions is

examined and compared with the widely used Soave-type and exponential forms, and the performance of these alpha functions on density estimation of representative substances, including oxygen, carbon dioxide, and n-decane, is discussed in detail. The calibrated alpha functions improve the estimation of density dramatically in all regions of the thermodynamic fluid states of the substances of interest, compared to empirical alpha functions.

The paper is organized as follows. Section 2 describes the theoretical formulation of the PR EOS, the statistical calibration technique, and the three proposed computer models. Section 3 examines the performance of the calibrated models and compare to empirical approaches. Finally, Section 4 presents conclusions.

2. Theoretical formulation

In this section, the problem of interest is first stated. We focus on the improvement of PR EOS due to its simple form and wide popularity. The statistical calibration method is then introduced to find a suitable functional form of the alpha function associated with optimal parameters. Since we will use physical data covering all thermodynamic regions, the alpha function is expected to be different from the Soave-type or exponential functions that have been extensively employed in other studies. Various alpha functions are explored with different numbers of variables and calibration parameters.

2.1. Peng-Robinson equation of state

Semiempirical cubic EOS generally express pressure (P) as the sum of two terms, a repulsion pressure P_R and an attraction pressure P_A, i.e., $P = P_R + P_A$. For typical cubic EOS, such as vdW, SRK, and PR equations, P_R and P_A can be expressed as

$$P_R = \frac{R_u T}{\bar{v} - b}$$
$$P_A = -\frac{a_c \alpha}{f(\bar{v})} \tag{1}$$

where $R_u, T,$ and $\bar{v}$ represents the universal gas constant, temperature, and molar volume, respectively. A general expression of $f(\bar{v})$ can be written as,

$$f(\bar{v}) = \bar{v}(\bar{v} + b) + c(\bar{v} - b). \tag{2}$$

The constant b is related to the size of the molecules, and the product $a_c\alpha$ is a measure of the intermolecular attraction force. a_c, b, and c are constants determined by critical point constraint, and α is called the alpha function. Combining Eqs. (1) and (2), a three-parameter EOS is obtained as follows,

$$P = \frac{RT}{v - b} - \frac{a_c \alpha}{v(v + b) + c(v - b)} \quad , \tag{3}$$

which is known as the Patel-Teja (PT) EOS [34]. The PT EOS is reduced to a two-parameter EOS when the parameter c is assigned as a special value. It reduces to the SRK EOS if $c = 0$ and to the PR EOS if $c = b$. Many studies have focused on finding a proper alpha function (α), such as the Soave-type alpha functions [8, 9] and exponential alpha functions [19, 22, 23, 35], which are empirical expressions of the reduced temperature (T_r), for example,

Soave function [9]: $$\alpha = \left[1 + F\left(1 - \sqrt{T_r}\right)\right]^2 \tag{4}$$

Gasem et al. function [19]: $$\alpha = \exp\left[(G_1 + G_2 T_r)\left(1 - T_r^{G_3}\right)\right], \tag{5}$$

where the modeling parameters (F, G_1, G_2, G_3) were determined by minimizing an objective function. The objective function could be the relative error of the property of interest, or least-

squares error in a limited range of saturation temperatures. As mentioned earlier, these alpha functions exhibit poor performances in the compressed liquid, near-critical point, and supercritical fluid regions, because of the lack of physical data in these regions and the *ad hoc* optimization technique for parameter estimation.

To this end, we intend to develop an alpha function suitable for a much broader range of thermodynamic states and leverage the statistical calibration technique. We choose the two-parameter PR EOS as the benchmark of the calibration for several reasons. First, two-parameter EOS have simpler formulas and are much easier to incorporate into multiphysics simulation frameworks. Second, the PR EOS representation of attractive pressure forces and critical compressibility factor is closer to those of hydrocarbons, as compared to the SRK EOS [7, 9]. The calibration technique described below, however, can be extended to the development of any EOS. The benefit of the proposed modified PR EOS in the present work is to minimize the required modification of existing multiphysics simulation frameworks, where the PR EOS is involved.

2.2. Calibration model

Calibration is a process of using outputs from physical experiments or high-fidelity simulations to learn and adjust the parameters of the computer model. In the calibration problem, there are two groups of input parameters: calibration parameters and variable parameters. Calibration parameters are the unknown context-specific inputs that we wish to learn about. These parameters are supposed to take fixed but unknown values $\boldsymbol{\theta} = (\theta_1, \dots, \theta_q)$ for all the observations to be used for calibration, and for all other instances that we plan to use the calibrated model to predict. Variable parameters have different but known values $\mathbf{x} = (x_1, \dots, x_d)$ for each of the

observations to be used for calibration. Their values are either known or subject to parametric variability for new predictions. We denote the scalar output of the computer model as a function of variable parameters $\mathbf{x}$ and calibration parameters $\boldsymbol{\theta}$ by $f(\mathbf{x};\boldsymbol{\theta})$. The observation of the real process with the variable parameters $\mathbf{x}$ is denoted by $y(\mathbf{x})$. Our objective is to find the best calibration parameters to minimize the difference between the computer model and the physical data.

2.2.1. Model specification

In the context of the current problem, we will propose several model forms of the alpha function with different calibration parameters, and quantify their uncertainties. Since we do not know the true alpha values, we consider the derived results from the standard NIST database [13] as the observations $y(\mathbf{x}_i)$, where $i = 1, \dots, n$ and n is the number of observations for the calibration process. Following Eq. (3), the alpha of PR EOS can be expressed as a function of pressure, temperature and molar volume.

$$\alpha = \left(\frac{RT}{v-b} - P\right)\frac{(v^2 + 2bv - b^2)}{a_c}. \tag{6}$$

According to the state postulate, only two of the three intensive properties are independent. If pressure and temperature are selected, the corresponding molar volume can be retrieved from the NIST database. Following this idea, we may consider both temperature and pressure as variable parameters in the computer model of the alpha function. In the current literature, however, only temperature is included as a variable parameter for pure substance. We will consider both scenarios and discuss why the two variable parameters are necessary for the best prediction of alpha values and subsequent density estimation.

Figure 1 shows an example of oxygen alpha values retrieved from the NIST database using Eq. (6), together with the calculated results from the Soave-type and Gasem et al. functions over wide ranges of temperature and pressure. Here $F = 0.415419, G_1 = 1.943, G_2 = 0.926$, and $G_3 = 0.1441$ for oxygen [23]. Large differences between the NIST derived values and the empirical counterparts (Soave-type and exponential functions) are observed. As the pressure varies from subcritical to supercritical values, the alpha curves merge into a single curve at high temperature. However, at low and intermediate temperature, alpha shows significant sensitivity to pressure change. The empirical alpha functions were developed using mainly the data in the liquid-vapor saturation region, denoted by the red enclosed area in Fig. 2. The thermodynamic fluid states can be generally partitioned into four regions: compressed liquid, liquid-vapor saturation, gas, and supercritical fluid regions. Implementation of empirical alpha functions to the areas outside of liquid-vapor saturation region may cause large error in density estimation, given the disparity among alphas at different pressures in Fig.1. The purpose of this work is to develop an alpha function that is suitable to all of the thermodynamic fluid regions in Fig. 2; for statistical learning the observational dataset must sweep variable parameters across all fluid states.

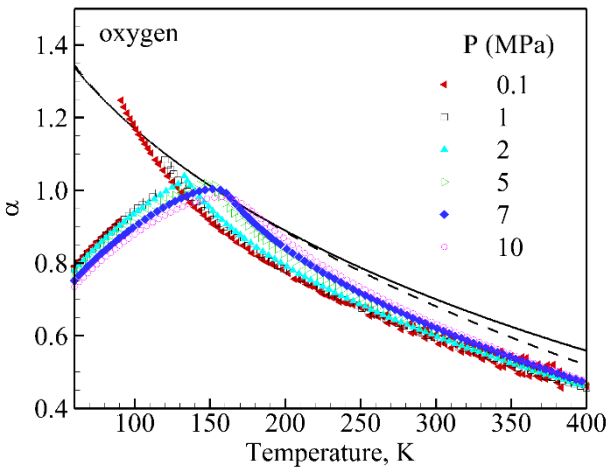

Fig. 1. Alpha values of oxygen retrieved from the NIST database (symbols) and calculated by Soave (solid line) and exponential (dashed line) functions over wide ranges of temperature and pressure

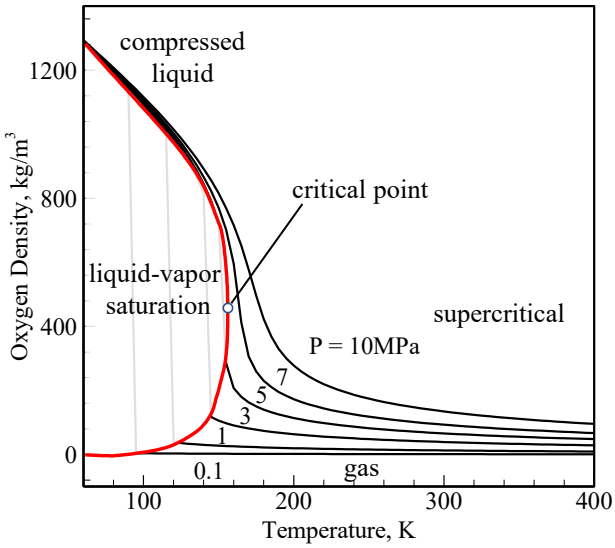

Fig. 2. Density-temperature phase diagram of oxygen

The physical data retrieved from the NIST database inherently contain uncertainty, which can come from measurement error embedded in the database or calculation error during the data retrieval process. In the present work, we call this type of error simply measurement error ϵ_i for each observation, and the relation between the physical reality and observation is written as

$$y(\mathbf{x}_i) = f(\mathbf{x}_i; \boldsymbol{\theta}) + b_{\boldsymbol{\theta}}(\mathbf{x}_i) + \epsilon_i. \tag{7}$$

Here ϵ_i is interpreted as stochastic error in the NIST database and is assumed to independently and identically follow a normal distribution with zero mean and variance $\mathbb{V}[\epsilon_i] = \sigma^2$. In addition, the bias between the computer model and the physical reality, denoted by $b_{\boldsymbol{\theta}}(\mathbf{x}_i)$ in Eq (7), must be defined. The dependence of $b_{\boldsymbol{\theta}}(\mathbf{x}_i)$ on $\boldsymbol{\theta}$ is often suppressed in the literature [27], but it is included here for clarity. The advantage of the present calibration model is the inclusion of model bias, since the truth is generally unknown and the trained model is inexact. In other words, the

computer model does not perfectly match physical reality, even with an optimal calibration parameter, and it is thus necessary to include the contribution of the bias as the part of the predictor (or bias-corrected predictor).

The model bias $b_{\boldsymbol{\theta}}(\cdot)$ is typically modeled with a Gaussian process (GP), which assumes that the joint distribution of $b_{\boldsymbol{\theta}}(\mathbf{x}_1), \ldots, b_{\boldsymbol{\theta}}(\mathbf{x}_n)$ is a multivariate normal distribution with zero mean and a positive-definite covariance matrix, each element of which is calculated by a covariance function. This covariance function is typically expressed by $\nu k(\mathbf{x}_i, \mathbf{x}_j)$, where $\nu > 0$ is the process variance and $k(\mathbf{x}_i, \mathbf{x}_j)$ is a kernel function with $k(\mathbf{x}_i, \mathbf{x}_i) = 1$ for any $\mathbf{x}_i$. A typical choice of the kernel is a Gaussian kernel that has the form $k(\mathbf{x}_i, \mathbf{x}_j) = \exp(-\gamma \|\mathbf{x}_i - \mathbf{x}_j\|^2)$, where $\gamma > 0$ is an unknown parameter. Recent studies [26, 27], however, showed that these kernel functions may cause unidentifiability of the calibration parameters. To remedy this issue, the orthogonal kernel function has been proposed [27]. Therefore, we assume that the model bias $b_\theta(\cdot)$ is a GP with zero mean and an orthogonal kernel function following the form,

$$k(\mathbf{x}_i, \mathbf{x}_j) = k_0(\mathbf{x}_i, \mathbf{x}_j) - h_{\boldsymbol{\theta}}(\mathbf{x}_i)^T H_{\boldsymbol{\theta}}^{-1} h_{\boldsymbol{\theta}}(\mathbf{x}_j), \tag{8}$$

where k_0 is a Gaussian kernel, i.e., $k_0(\mathbf{x}_i, \mathbf{x}_j) = \exp(-\gamma \|\mathbf{x}_i - \mathbf{x}_j\|^2)$, and

$$h_{\boldsymbol{\theta}}(\mathbf{x}) = \int_{\chi} \frac{\partial}{\partial \boldsymbol{\theta}} f(\boldsymbol{\xi}, \boldsymbol{\theta}) k_0(\mathbf{x}, \boldsymbol{\xi}) d\boldsymbol{\xi}, \tag{9}$$

$$H_{\boldsymbol{\theta}} = \int_{\chi} \int_{\chi} \frac{\partial}{\partial \boldsymbol{\theta}} f(\boldsymbol{\xi}_1, \boldsymbol{\theta}) \left(\frac{\partial}{\partial \boldsymbol{\theta}} f(\boldsymbol{\xi}_2, \boldsymbol{\theta}) \right)^T k_0(\boldsymbol{\xi}_1, \boldsymbol{\xi}_2) d\boldsymbol{\xi}_1 d\boldsymbol{\xi}_2, \tag{10}$$

where χ is the design range of variable parameters. The integrals in Eqs. (9) and (10) can be performed through a stochastic average approximation, such as Monte Carlo sampling [36]. In the

present problem, the proposed model functions $f(\mathbf{x}, \boldsymbol{\theta})$ are relatively simple and the corresponding gradient is obtainable, as will be shown later.

With the GP modeling, the observations, denoted by $Y_n = \left(y(\mathbf{x}_1), y(\mathbf{x}_2), \dots, y(\mathbf{x}_n)\right)^T$, follow a multivariate normal distribution,

$$Y_n \sim N(\mathbf{f}_n(\boldsymbol{\theta}), \nu\mathbf{K}_n + \sigma^2\mathbf{I}_n), \tag{11}$$

where $\mathbf{f}_n(\theta) = \left(f(\mathbf{x}_1, \boldsymbol{\theta}), f(\mathbf{x}_2, \boldsymbol{\theta}), \dots, f(\mathbf{x}_n, \boldsymbol{\theta})\right)^T$, $\mathbf{K}_n$ is an $n \times n$ matrix and the (i, j) element is $k(\mathbf{x}_i, \mathbf{x}_j)$, and $\mathbf{I}_n$ is an $n \times n$ identity matrix. Given the parameters $\boldsymbol{\theta}, \nu, \gamma$, and σ^2 and the observations Y_n, the predictive distribution of $y(\mathbf{x})$ at new inputs $\mathbf{x}_{\text{new}}$, that is, $y(\mathbf{x}_{\text{new}})|Y_n$, follows a normal distribution $N(\mu(\mathbf{x}_{\text{new}}), \sigma^2(\mathbf{x}_{\text{new}}))$, where the mean and variance can be derived from the property of multivariate normal distribution, which can be expressed, respectively, as

$$\mu(\mathbf{x}_{\text{new}}) = f(\mathbf{x}_{\text{new}}, \boldsymbol{\theta}) + \mathbf{k}_n(\mathbf{x}_{\text{new}})^T \left(\mathbf{K}_n + \frac{\sigma^2}{\nu}\mathbf{I}_n\right)^{-1} \left(Y_n - \mathbf{f}_n(\boldsymbol{\theta})\right), \tag{12}$$

and

$$\sigma^2(\mathbf{x}_{\text{new}}) = \nu + \sigma^2 - \nu\mathbf{k}_n(\mathbf{x}_{\text{new}})^T \left(\mathbf{K}_n + \frac{\sigma^2}{\nu}\mathbf{I}_n\right)^{-1} \mathbf{k}_n(\mathbf{x}_{\text{new}}), \tag{13}$$

where $\mathbf{k}_n(\mathbf{x}_{\text{new}}) = \left(k(\mathbf{x}_{\text{new}}, \mathbf{x}_1), \dots, k(\mathbf{x}_{\text{new}}, \mathbf{x}_n)\right)^T$. The unknown parameters can be obtained by maximum likelihood estimation that is introduced in the next subsection. $\mu(\mathbf{x}_{\text{new}})$ can be considered as the predictor of the alpha function at the new variable setting, which is essentially the sum of the model function and a correction for observation error and model discrepancy. Such a correction is crucial for the more accurate capture of the physical reality. Since our predictor consists of a deterministic part (computer model) and a statistical correction (model bias), we regard our calibration model as a *semi-parametric alpha function*. Another highlight of the current

calibration model is the automatic uncertainty quantification by $\sigma^2(\mathbf{x}_{\text{new}})$. It is easy to verify that when $\mathbf{x}_{\text{new}}$ coincides one of the variable settings in the training dataset and the measurement error σ^2 is sufficiently small, the predictor $\mu(\mathbf{x}_{\text{new}})$ approaches the corresponding observation. In other words, the predictor can accurately recover all training points without the introduction of additional error, unlike the conventional regression methods used in the literature on EOS development.

2.2.4. Parameter estimation

The calibration model includes the unknown parameters $\boldsymbol{\theta}, \nu, \gamma$, and σ^2, which need to be estimated. Here we adopt the maximum likelihood estimation (MLE) method. The log-likelihood of the parameters is

$$l = \text{constant} - \frac{1}{2}\log|\nu\mathbf{K}_n + \sigma^2\mathbf{I}_n| - \frac{1}{2}\big(Y_n - \mathbf{f}_n(\boldsymbol{\theta})\big)^T(\nu\mathbf{K}_n + \sigma^2\mathbf{I}_n)^{-1}\big(Y_n - \mathbf{f}_n(\boldsymbol{\theta})\big). \tag{14}$$

Similar to [37], let $g = \sigma^2/\nu$ and regard it as a new parameter that replaces σ^2. Then, conditioned on g, θ and γ, the MLE $\hat{v}$ has a closed form

$$\hat{v} = \frac{1}{n}\big(Y_n - \mathbf{f}_n(\boldsymbol{\theta})\big)^T(\mathbf{K}_n + g\mathbf{I}_n)^{-1}\big(Y_n - \mathbf{f}_n(\boldsymbol{\theta})\big). \tag{15}$$

Plug $\hat{v}$ back into the log-likelihood, we get a profile log-likelihood involving just the remaining parameters g, θ and γ, which is

$$l(g, \theta, \gamma) = \text{constant} - \frac{1}{2}\log|\mathbf{K}_n + g\mathbf{I}_n| - \frac{n}{2}\big(Y_n - \mathbf{f}_n(\boldsymbol{\theta})\big)^T(\mathbf{K}_n + g\mathbf{I}_n)^{-1}\big(Y_n - \mathbf{f}_n(\boldsymbol{\theta})\big). \tag{16}$$

The MLEs of g, θ, γ, unfortunately, do not have a closed form, but they can be obtained by numerical methods. A quasi-Newton optimization method [37, 38] is adopted here to find the MLEs $\hat{g}, \hat{\theta}, \hat{\gamma}$ by maximizing the log-likelihood numerically.

2.3. Selection of computer models

As discussed previously, the mathematical model of the real alpha function is unknown, and the proposed computer models only tend to approach the reality. The calibration model represented by Eq. (12) gives a predictor as the sum of the computer model and a correction due to model discrepancy and measurement error. This implies that the bias correction can compensate for the uncertainty of the computer model to the predictor. In the present work, we examine three computer models with different variable and calibration parameters as follows,

$$\text{Model 1: } f_1(T_r;\theta) = c + \theta^{(1)}T_r, \tag{17}$$

$$\text{Model 2: } f_2(T_r;\theta_1,\theta_2) = \theta_1^{(2)} + \theta_2^{(2)}T_r, \tag{18}$$

$$\text{Model 3: } f_3(T_r,P_r;\theta_1,\theta_2,\theta_3) = \theta_1^{(3)} + \theta_2^{(3)}T_r + \theta_3^{(3)}P_r. \tag{19}$$

Here c, T_r, and P_r represent the *ad hoc* constant, reduced temperature ($T_r = T/T_c$), and reduced pressure ($P_r = P/P_c$), respectively. Both computer models 1 and 2 have reduced temperature as the variable parameter. Model 2 has two calibration parameters, as compared to model 1 which has one. Computer model 3 includes reduced pressure as the second variable parameter associated with the third calibration parameter. This selection is justified by Fig. 1, which shows the strong dependence of alpha on pressure in some regions. Note that the alpha function presents nonlinear behaviors, although linear models are employed here for the convenience of gradient term calculations involved in the kernel function. The uncertainty induced by the linear models can be compensated by the bias-corrected term in Eq. (12). As will be seen later, this semi-parametric form shows superior performance in the prediction of alpha and density estimation of substances at all thermodynamic states.

3. Results and discussion

We select three representative substances, oxygen, n-decane, and carbon dioxide, and develop their alpha functions based on the proposed model forms to illustrate the calibration model. The phase-change properties of these substances are listed in Table 1. The alpha distribution of oxygen is shown in Fig. 1. Figure 3 shows the alpha values of n-decane and carbon dioxide at different thermodynamic states, as retrieved from the NIST database. Pressure-dependent behavior is also observed for n-decane and carbon dioxide. As discussed earlier, the empirical alpha functions were obtained using data from only the liquid-vapor saturation region, and they are therefore expected to show poor performance in the regions of compressed liquid, near-critical point, and supercritical fluid. The proposed semi-parametric alpha functions are examined in detail with the Soave and exponential alpha functions.

Table 1 Thermodynamic properties of representative substances

Substance	critical temperature (T_c, K)	critical pressure (P_c, MPa)	normal boiling temperature (T_b, K)
oxygen	154.58	5.04	90.2
n-decane	617.8	2.11	447.2
carbon dioxide	304.18	7.38	216.58*

*triple point temperature where pressure is 0.518 MPa

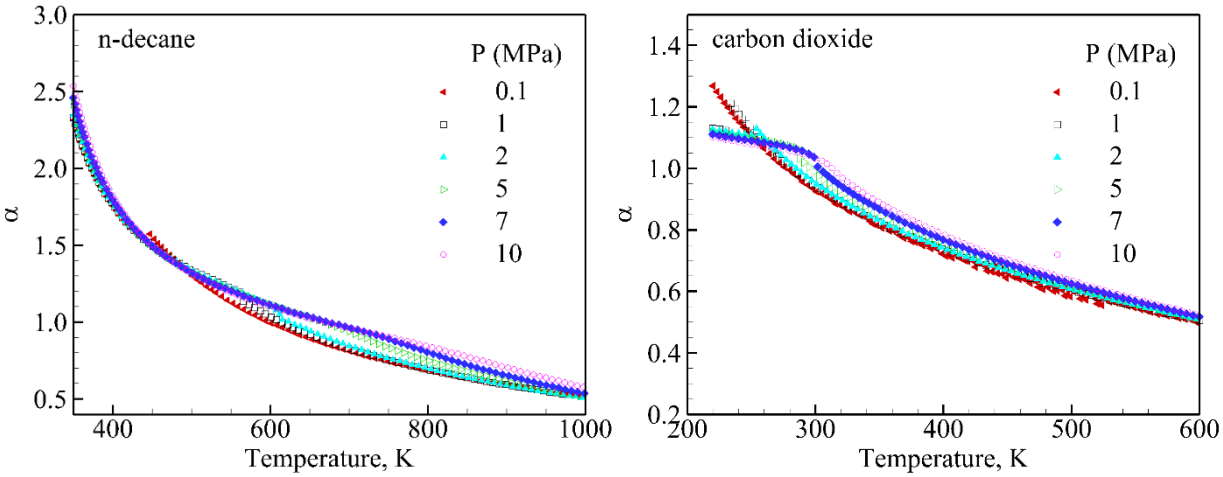

Fig. 3. Alpha values of n-decane and carbon dioxide retrieved from the NIST database for wide ranges of temperature and pressure

3.1. Comparison with empirical models

Figure 4 presents a comparison of calibrated models with and without model bias, using Model 1, Model 2, Soave, and Gasem et al. (Exponential). The common feature of these models is that the reduced temperature ($T_r = T/T_c$) is the only variable parameter. The training data include a T_r range from 0.4 to 2.6 and three P_r ($P_r = P/P_c$) values (0.2, 1.0, 1.98). The different pressure inputs are treated as sample observations at a given T_r. Since the earlier parameter estimation for the Soave and exponential alpha functions excluded data from outside of the saturation region, the parameters F and G_3 are recalibrated using the present technique with the same dataset. The results show that all of the models without bias correction are nearly linear and that the larger model errors for the Soave and Gasem et al. functions appear in the low temperature zone (T_r<1, compressed liquid region). The predictions with bias correction, represented by black solid lines, are consistently accurate, regardless of model form. This highlights the importance of model bias in the prediction of alpha function, especially when the model form is inexact.

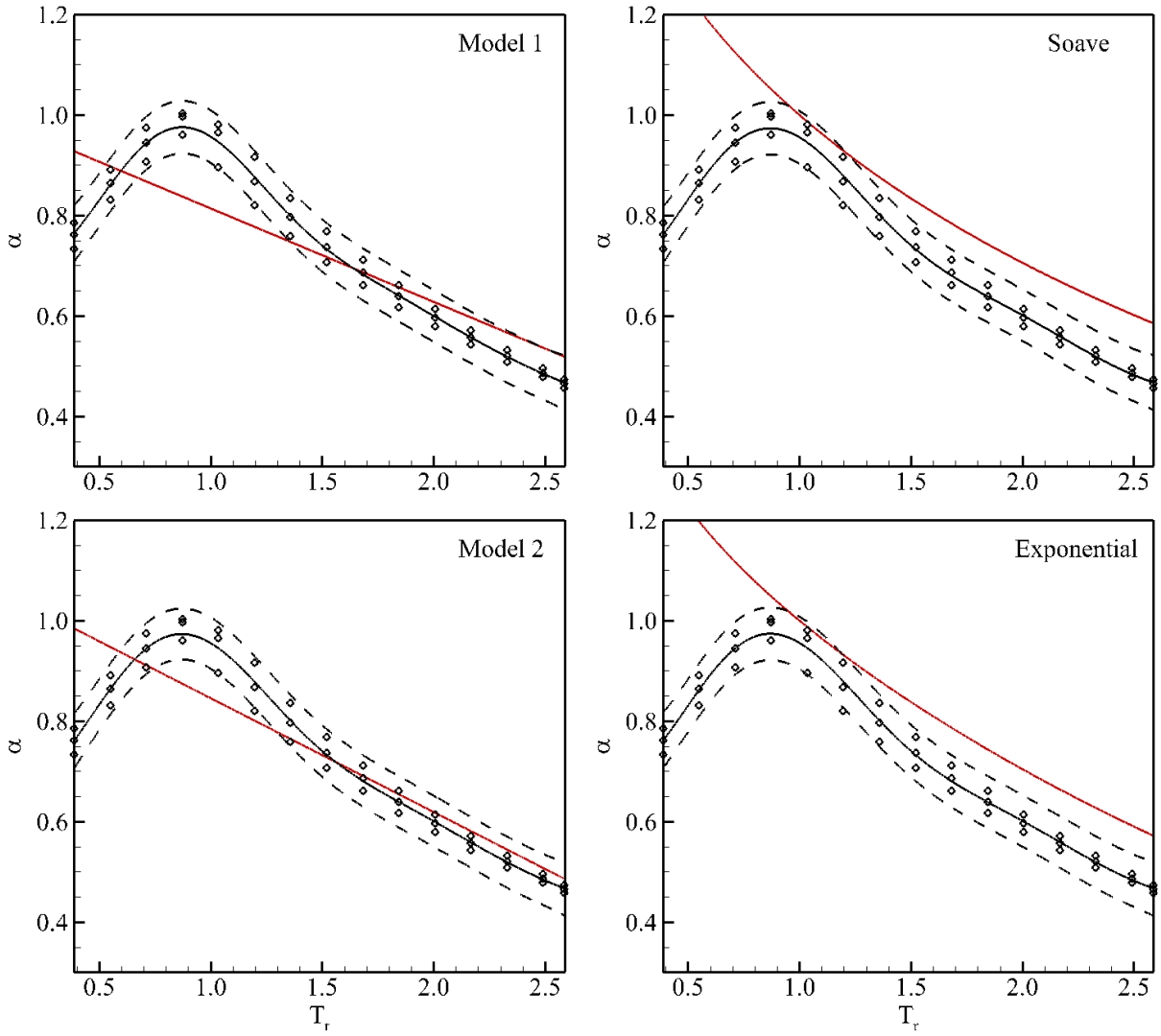

Fig. 4. Calibrated models for oxygen alpha functions: (1) pure computer model (red solid lines); (2) bias-corrected model predictors (black solid lines); (3) training data derived from the NIST database (circles); and (4) 95% tolerance bounds (dashed lines)

The optimal values of the calibration parameters in Model 1, Model 2, Soave, and Exponential are $\hat{\theta}^{(1)} = -0.1858$, $(\hat{\theta}_1^{(2)}, \hat{\theta}_2^{(2)}) = (1.0723, -0.2265)$, $\hat{F} = 0.3856$, and $\hat{G}_3 = 0.1273$, respectively. Here the intercept (c) of Model 1 is adjusted in an *ad hoc* way with a value of 0.62. The optimal values of F and G_3 turn out to differ from those in the literature [23]. Although all of the bias-corrected models show promising predictions, minimum bias correction is desirable. To

determine which model is favorable, Fig. 5 shows the contribution of model bias to the prediction for all models. The Soave and Exponential models show higher weight of the model bias in the low- and high-temperature ranges, except in the region near T_r=1 and Model 2 shows overall low contribution of the model bias compared to Model 1. The latter may be because the calibrated intercept $\theta_1^{(2)}$ from the training data in Model 2 is superior to the *ad hoc* value used in Model 1. In summary, the present calibration model can capture the trend of the alpha function in a reasonable way using all these models with a single variable parameter, and Model 2 gives the overall best model accuracy with the lowest bias contribution. Model 2 is selected as the representative one-variable parameter model for the subsequent discussion.

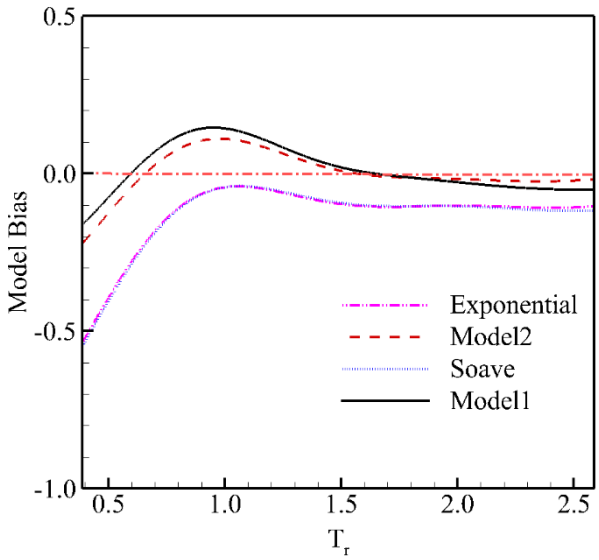

Fig. 5. Contribution of model bias to the prediction for all models (Dash-dotted line is reference of zero model bias)

3.2. Performance of Model 2

3.2.1. Prediction of alpha function

In this section, we explore in more detail the performance of Model 2 in the prediction of the alpha functions of representative substances. As shown in Fig. 4, alpha in the sample data changes

substantially as the reduced pressure varies from 0.1 to 1.98 at a given temperature. This induces a large variance in the measurement error, and reduces the accuracy of the pure computer model. To alleviate the situation, we narrow the range of the reduced pressure for the estimation of the sample variance.

Figures 6-8 show the calibrated models associated with the model bias using Model 2 for oxygen, n-decane, and carbon dioxide, respectively. Non-monotonic change of the alpha function occurs for oxygen while a monotonic decrease occurs for both n-decane and carbon dioxide. The pure computer models denoted by red solid lines are determined by calibrating the optimal parameters. The calibrated slope ($\hat{\theta}_2^{(2)}$) is negative for all substances. The pure models present large discrepancies from the sample data at the turning points for all substances. This observation is aligned with the magnitude of the model bias, which complements the uncertainty of the pure models. The trend of the alpha function for carbon dioxide is closer to linear with overall smaller bias, compared to the other two substances. The bias-corrected predictions represented by the black solid lines closely capture the general variation of alpha functions for all substances with negligible visual difference.

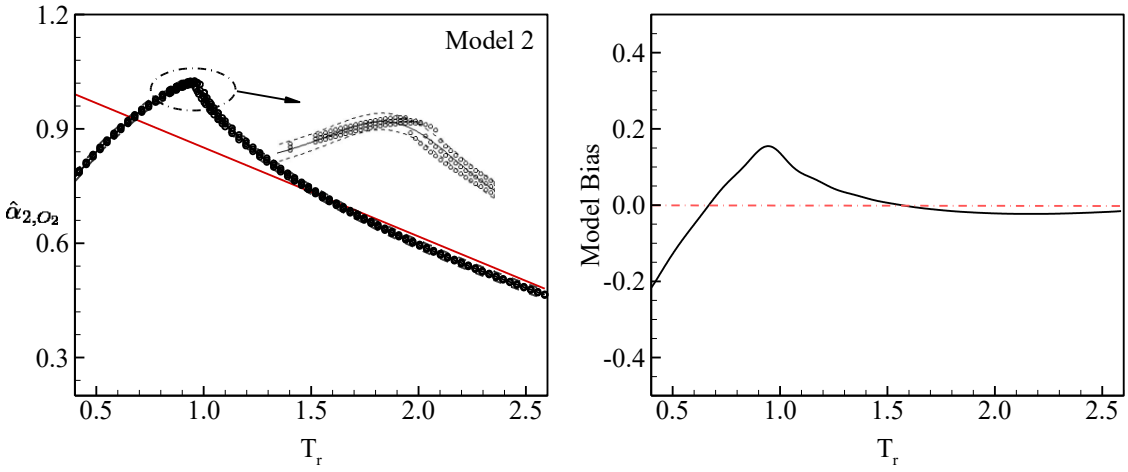

Fig. 6. Calibrated alpha function (top) and model bias (bottom) for oxygen using Model 2: $(\hat{\theta}_1^{(2)}, \hat{\theta}_2^{(2)})$=(1.084245, -0.2332414) with three $\boldsymbol{P_r}$ values (0.8. 0.9, and 1.0).

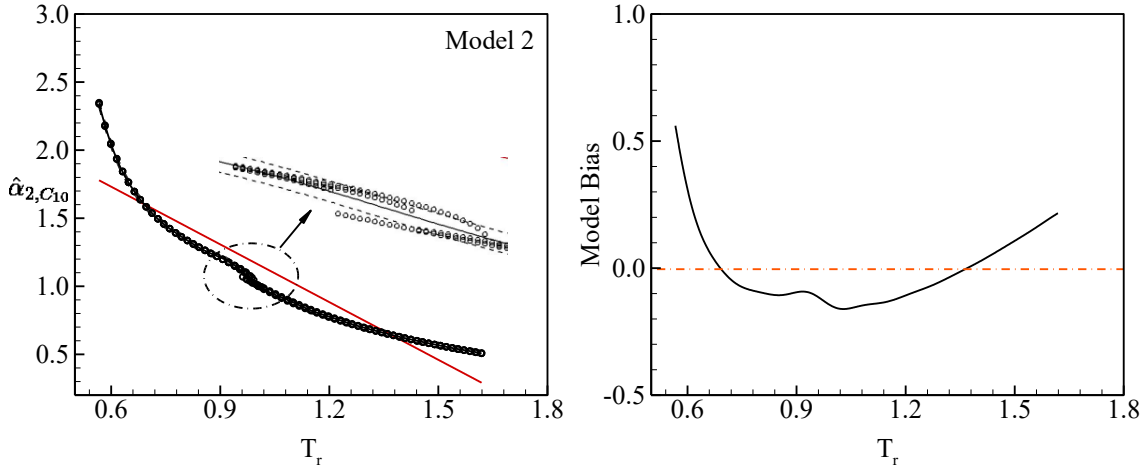

Fig. 7. Calibrated alpha function (top) and model bias (bottom) for n-decane using Model 2: $(\hat{\theta}_1^{(2)}, \hat{\theta}_2^{(2)})$=(2.579569, -1.413308) with three $\boldsymbol{P_r}$ values (0.05. 0.71, and 0.95).

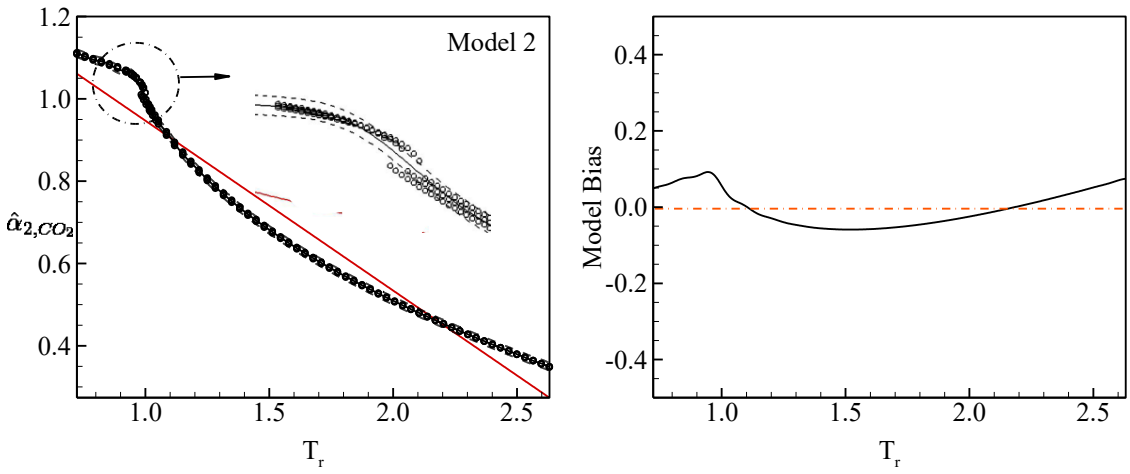

Fig. 8. Calibrated alpha function (top) and model bias (bottom) for carbon dioxide using Model 2: $(\hat{\theta}_1^{(2)}, \hat{\theta}_2^{(2)})$=(1.359819, -0.4127742) with three $\boldsymbol{P_r}$ values (0.82. 0.89, and 0.95).

3.2.2. Density estimation

The goal of calibrating the alpha function is to configure a robust PR EOS that can predict the density of a substance at all thermodynamic fluid states in a faithful manner. The modified PR EOS is expressed in Eq. (3) together with the calibrated semi-parametric alpha function ($\hat{\alpha}_2$). Figure 9 shows the evaluated density (solid lines) for oxygen using the modified PR EOS over wide ranges of temperature and pressure. For comparison, the density retrieved from the NIST database (symbols) and evaluated by the Soave function (dashed lines) is also included. The vertical lines denote the phase change from liquid (high density) to gas (low density) at subcritical pressure ($P < 5.04$ MPa). This sharp change in density becomes a smooth density variation at supercritical pressure (7MPa, 10 MPa), where the high density gradient region corresponds to the region of transition from compressed liquid to supercritical fluid [39]. The empirical PR EOS with the Soave alpha function overestimates density under low-temperature conditions, where compressed liquid is present. The modified PR EOS with the semi-parametric alpha function, on the other hand, substantially improves the density estimation in the liquid phase.

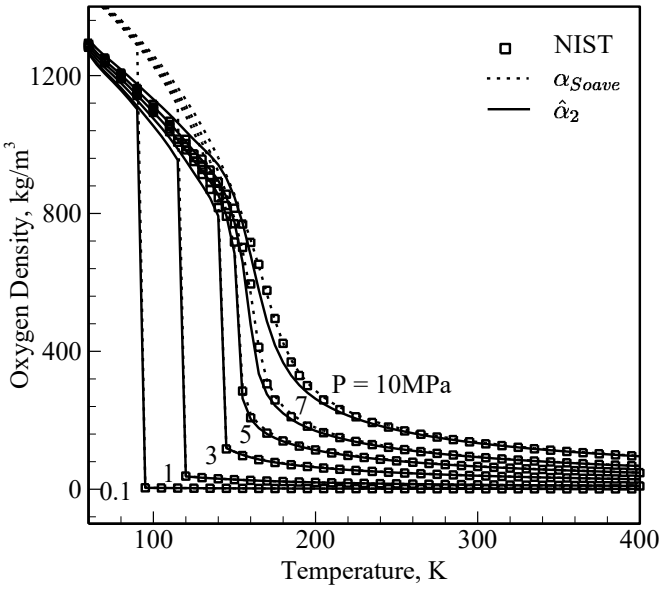

Fig. 9. Estimated density of oxygen using different approaches over wide ranges of temperature and pressure: (1) semi-parametric alpha function ($\hat{\boldsymbol{\alpha}}_{\mathbf{2}}$-solid lines); (2) Soave alpha function (dashed lines); and (3) NIST dataset (symbols)

Density predicted by both alpha functions shows close agreement with the NIST dataset under high-temperature and low-pressure conditions, where oxygen is in the gaseous state and the EOS is relatively insensitive to the magnitude of the alpha value. Gaseous oxygen has low density and large molar volume, which leads to a much smaller attractive pressure compared to the repulsive pressure, since the attractive pressure in the PR EOS is inversely proportional to the square of the molar volume. The alpha value difference between the Soave function and semi-parametric function causes negligible error due to the insignificant contribution of the attractive pressure to the PR EOS. When the attractive pressure approaches zero, the PR EOS approaches ideal-gas behavior.

At subcritical pressure, both alpha functions capture the position of the liquid-gas interface accurately. The semi-parametric function provides much better density estimation of saturated

liquid than the Soave function. At supercritical pressure, however, the Soave function outperforms the semi-parametric function for oxygen in the estimation of density in the transition region. This may be explained by the abnormal change of alpha values in the zoomed-in view shown in Fig. 6. The uncertainty in this region is relatively high. A small change in pressure can cause a large fluctuation in alpha and density. This suggests the impact of pressure on the accurate estimation of density in the transition region, which is included in Model 3 and discussed in the next section.

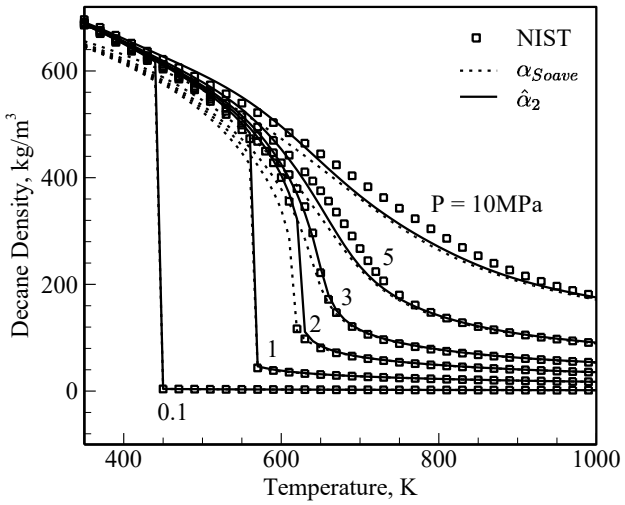

Fig. 10. Estimated density of n-decane using different approaches over wide ranges of temperature and pressure: (1) semi-parametric alpha function ($\hat{\boldsymbol{\alpha}}_{\mathbf{2}}$-solid lines); (2) Soave alpha function (dashed lines); and (3) NIST dataset (symbols)

Figure 10 presents the estimated density of n-decane using different approaches. Unlike the situation for oxygen, here the empirical PR EOS with the Soave function consistently underestimates the density at all thermodynamic states, except for the gas-like state, at which the density is insensitive to the alpha variation. The modified PR EOS with the semi-parametric alpha function improves the density prediction throughout all of the thermodynamic regimes. The most

substantial improvement occurs at the compressed-liquid state, while only limited improvement is achieved in the liquid-to-supercritical transition region.

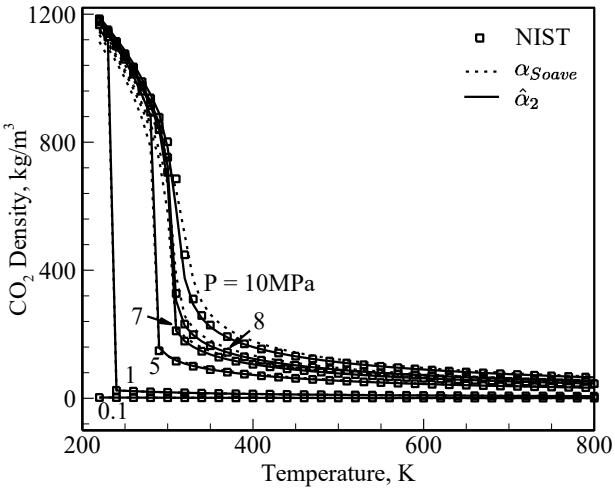

Fig. 11. Estimated density of carbon dioxide using different approaches over wide ranges of temperature and pressure: (1) semi-parametric alpha function ($\hat{\boldsymbol{\alpha}}_{\mathbf{2}}$-solid lines); (2) Soave alpha function (dashed lines); and (3) NIST dataset (symbols)

Figure 11 shows the estimated density of carbon dioxide using different approaches. The empirical PR EOS first underpredicts the density at compressed-liquid state, and then over-predicts the density in the transition region at supercritical pressure (P=8 MPa, 10 MPa). The density predicted by the modified PR EOS matches the NIST result very well for all thermodynamic states of carbon dioxide. Such excellent performance for carbon dioxide may be explained by the approximately linear trend of alpha embedded in the observational data and the resulting relatively smaller adjustment by the model bias.

3.3. Performance of Model 3

The semi-parametric alpha function developed using Model 2 shows poor density prediction at supercritical pressure, especially in the liquid-to-supercritical transition region, due to the high sensitivity of alpha to pressure. A new semi-parametric alpha function is therefore calibrated using Model 3 with three calibration parameters. Figures 12-14 show the comparison of $\hat{\alpha}_3$ and the NIST counterpart for the three substances. The two-dimensional contours of alpha present the influence of pressure in the vicinity of critical temperature (T_r=1) for all substances. The iso-contours of alpha lean to the right with increasing pressure, so it is necessary to consider this pressure effect to correctly capture the alpha variation in the near-critical temperature region. Visual comparison of alpha distributions shows that the semi-parametric alpha function $\hat{\alpha}_3$ faithfully emulates the NIST counterpart throughout the pressure-temperature space.

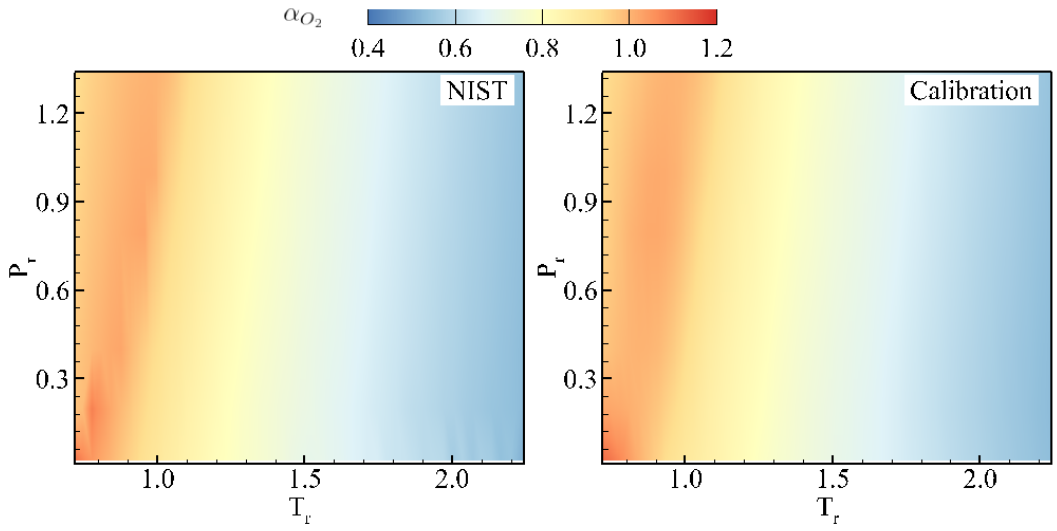

Fig. 12. Oxygen alpha distributions in pressure-temperature space; comparison of NIST result and $\hat{\boldsymbol{\alpha}}_{\mathbf{3}}$ with calibrated parameters: $(\hat{\theta}_1^{(3)}, \hat{\theta}_2^{(3)}, \hat{\theta}_3^{(3)})$=(1.0900, -0.2416, 0.01143)

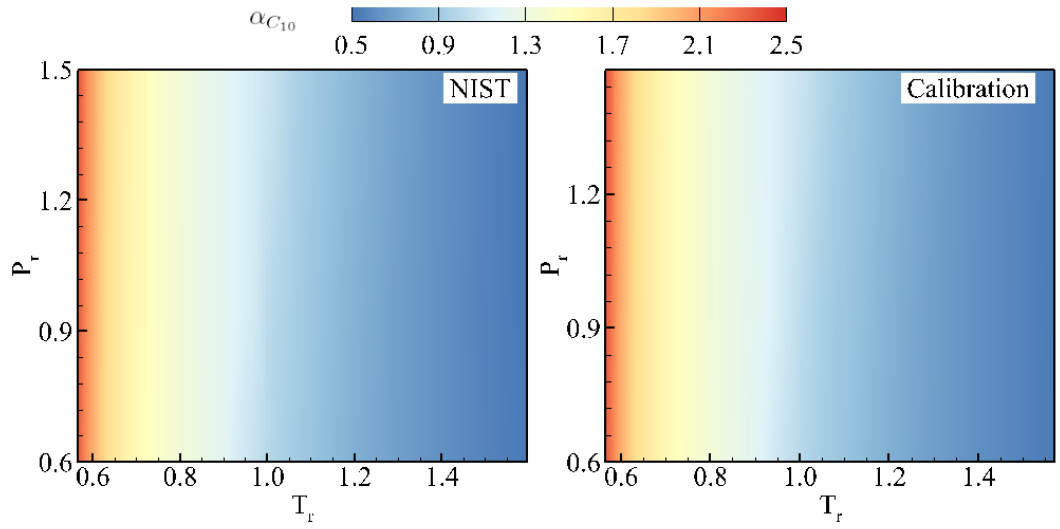

Fig. 13. N-decane alpha distribution in pressure-temperature space; comparison of NIST result and $\hat{\boldsymbol{\alpha}}_{\mathbf{3}}$ with calibrated parameters: $(\hat{\theta}_1^{(3)}, \hat{\theta}_2^{(3)}, \hat{\theta}_3^{(3)})$=(0.6910, 0.1377, 0.1492)

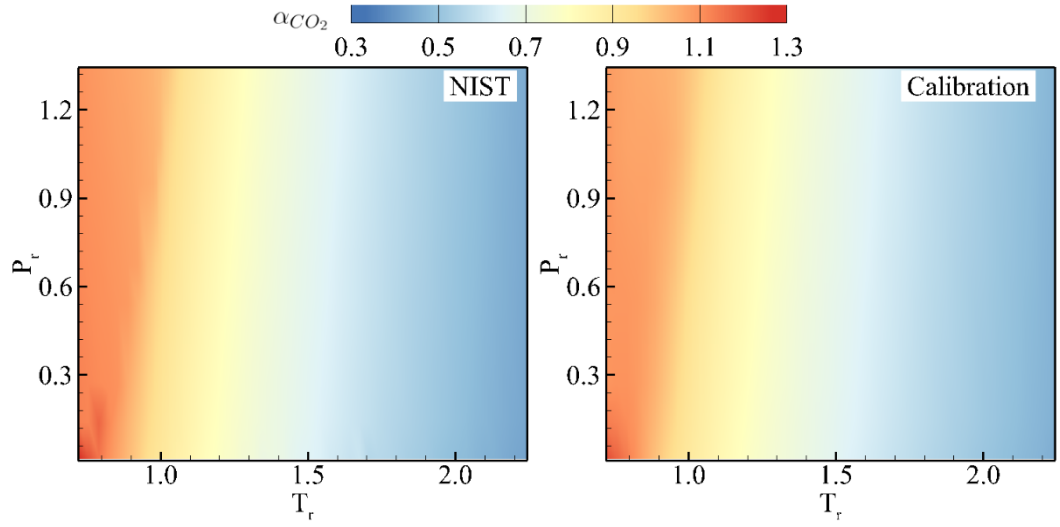

Fig. 14. CO_2 alpha distribution in pressure-temperature space; comparison of NIST result and $\hat{\boldsymbol{\alpha}}_{\mathbf{3}}$ with calibrated parameters: $(\hat{\theta}_1^{(3)}, \hat{\theta}_2^{(3)}, \hat{\theta}_3^{(3)})$=(1.3264, -0.4083, 0.02448)

The bias-corrected alpha function can be expressed as

$$\hat{\alpha}_3 = \hat{\theta}_1^{(3)} + \hat{\theta}_2^{(3)} T_r + \hat{\theta}_3^{(3)} P_r + bc \tag{20}$$

where bc is determined by the second term in Eq. (12) accounting for the correlation within the training data and the correlation between the training data and the unobserved data. Such a statistical treatment renders our calibration model to be semi-parametric. Figure 15 shows the distributions of relative error (RE) of the calibrated alpha for all substances at different temperature and pressure. RE of the present calibrated results is very small, with oxygen less than 5% and both n-decane and carbon dioxide less than 2%. Large RE occurs primarily at subcritical pressure for oxygen and carbon dioxide and in the near-critical region for n-decane. The effect of the RE in alpha on the estimation of density is discussed later.

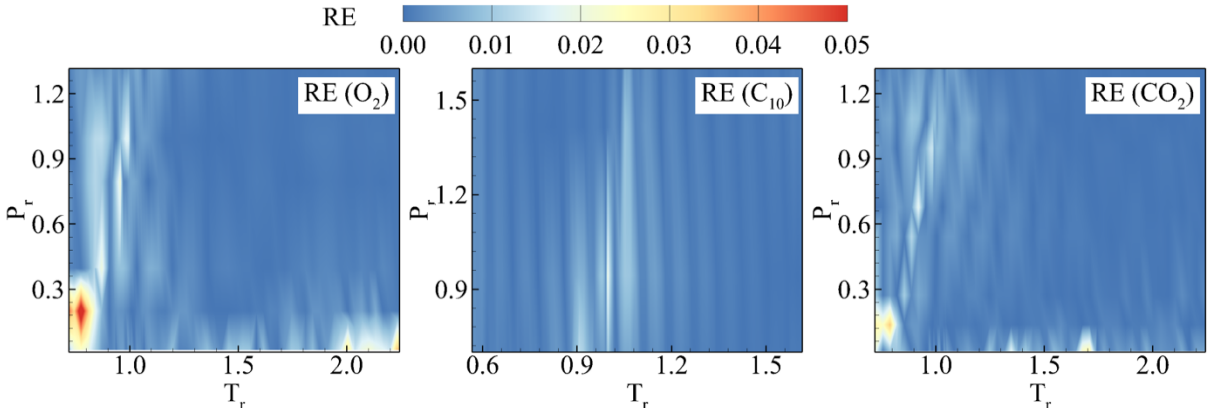

Fig.15. Distributions of relative error (RE) of predicted alpha for oxygen, n-decane, and carbon dioxide

Figures 16-18 show the calculated density using the modified PR EOS with $\hat{\alpha}_3$ (solid lines) at different temperature and pressure. The prediction accuracy is significantly improved, compared to $\hat{\alpha}_2$. The density distribution evaluated by the modified PR EOS is nearly overlapped with the NIST counterpart under all temperature and pressure conditions that cover all possible thermodynamic states. The alpha function $\hat{\alpha}_3$ predicts density very accurately at almost all thermodynamic states, including the underperformance regions in Model 2, that is, the liquid-to-supercritical transition and supercritical regions.

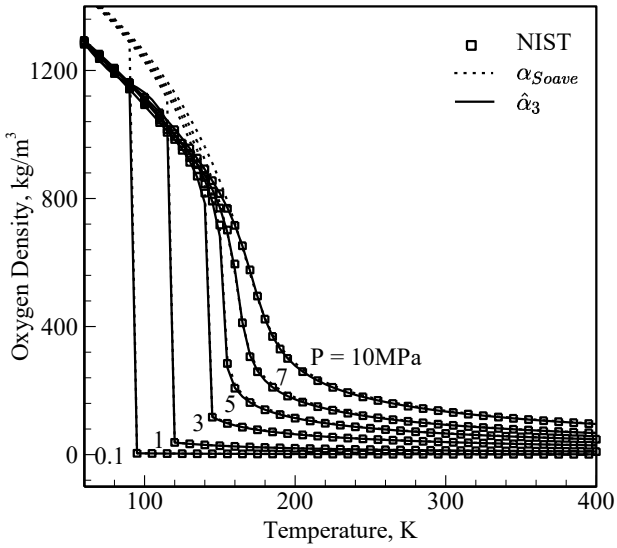

Fig. 16. Estimated density of oxygen using different approaches over wide ranges of temperature and pressure: (1) semi-parametric alpha function ($\widehat{\boldsymbol{\alpha}}_{\mathbf{3}}$-solid lines); (2) Soave alpha function (dashed lines); and (3) NIST dataset (symbols)

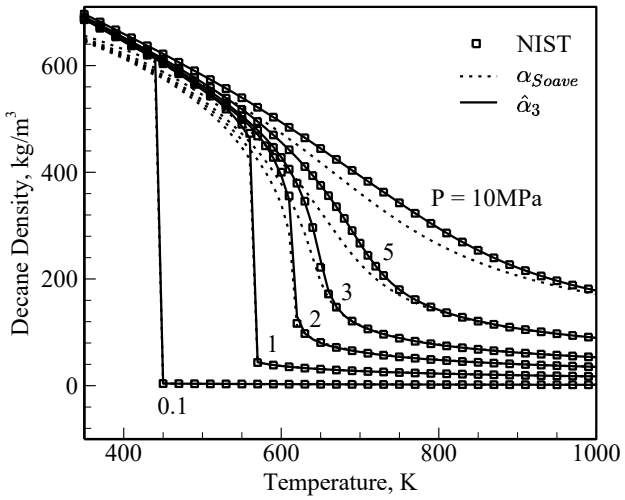

Fig. 17. Estimated density of n-decane using different approaches over wide ranges of temperature and pressure: (1) semi-parametric alpha function ($\widehat{\boldsymbol{\alpha}}_{\mathbf{3}}$-solid lines); (2) Soave alpha function (dashed lines); and (3) NIST dataset (symbols)

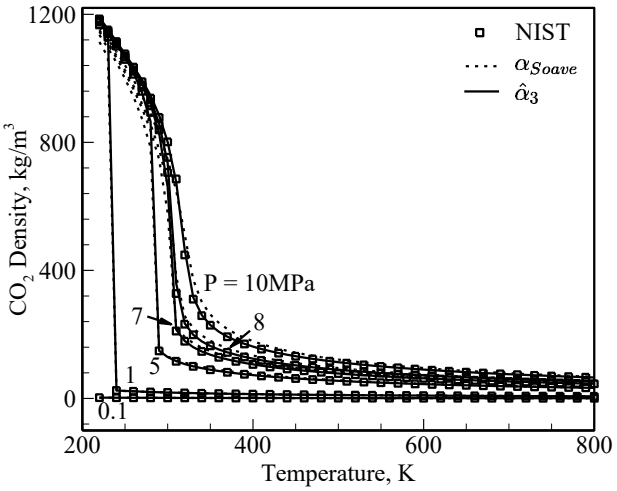

Fig. 18. Estimated density of carbon dioxide using different approaches over wide ranges of temperature and pressure: (1) semi-parametric alpha function ($\hat{\boldsymbol{\alpha}}_{\mathbf{3}}$-solid lines); (2) Soave alpha function (dashed lines); and (3) NIST dataset (symbols)

Figure 19 shows the variation of average relative error (ARE) of density using the Soave, $\hat{\alpha}_2$, and $\hat{\alpha}_3$ alpha functions at different pressure. The relative error is defined with respect to the NIST dataset, and ARE can be interpreted as the overall accuracy of estimation over all temperature conditions at a given pressure. The semi-parametric alpha function $\hat{\alpha}_3$ using Model 3 produces overall the smallest ARE (less than 0.5% everywhere) and is thereby the most accurate for estimation of density. The semi-parametric alpha function $\hat{\alpha}_2$ using Model 2 has a smaller ARE than the Soave function at all pressures, and ARE of both functions tend to be larger at higher pressure. This implies that $\hat{\alpha}_3$ should be adopted under high-pressure conditions, which are relevant to many contemporary propulsion and power-generation systems.

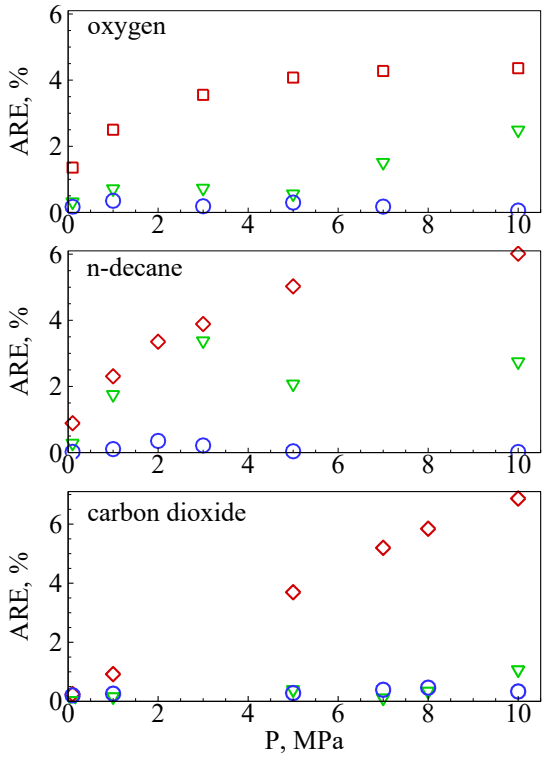

Fig. 19. Average relative error versus pressure in prediction of density by Soave function (squares) and semi-parametric functions using Model 2 (gradients) and Model 3 (circles) for all subject substances

4. Conclusion

The present study is motivated by the insufficient performance of empirical equations of state in the evaluation of volumetric behaviors and thermodynamic properties of fluids and fluid mixtures. We leverage recent advances in the calibration of inexact computer models and present a novel calibration technique to develop semi-parametric alpha functions that configure a modified Peng-Robinson equation of state. Semi-parametric alpha functions are constructed as the sum of a parametric computer model and a statistical correction accounting for model discrepancy. The latter is important to capture the faithful trend of alpha variation under different temperature and pressure conditions. Different model forms of the semi-parametric alpha function are explored and

compared with empirical Soave and exponential alpha functions. The accuracy of semi-parametric alpha functions is examined in detail for the prediction of the density of representative substances, including oxygen, n-decane, and carbon dioxide. Results show that the semi-parametric alpha function with two variable parameters and three calibration parameters provides consistently superior performance in the estimation of density over wide ranges of temperature and pressure at all thermodynamic states. The average relative error for the studied substances is below 0.5% at different pressures. The modified PR EOS maintains its simple cubic form and can be further implemented to compute other thermodynamic properties and study phase equilibrium for fluids and fluid mixtures, and it can be incorporated into large-scale multiphysics simulations where non-ideal gas behavior occurs.

5. References

[1] Oefelein, J.C. and V. Yang, "Modeling high-pressure mixing and combustion processes in liquid rocket engines," *Journal of Propulsion and Power*, Vol. 14, No. 5, 1998, pp. 843-857.

[2] Meng, H. and V. Yang, "A unified treatment of general fluid thermodynamics and its application to a preconditioning scheme," *Journal of Computational Physics*, Vol. 189, No. 1, 2003, pp. 277-304.

[3] Oefelein, J.C., "Large eddy simulation of turbulent combustion processes in propulsion and power systems," *Progress in Aerospace Sciences*, Vol. 42, No. 1, 2006, pp. 2-37.

[4] Wang, X., H. Huo, U. Unnikrishnan, and V. Yang, "A systematic approach to high-fidelity modeling and efficient simulation of supercritical fluid mixing and combustion," *Combustion and Flame*, Vol. 195, No., 2018, pp. 203-215.

[5] Wei, Y.S. and R.J. Sadus, "Equations of state for the calculation of fluid-phase equilibria," *AIChE Journal*, Vol. 46, No. 1, 2000, pp. 169-196.

[6] Valderrama, J.O., "The state of the cubic equations of state," *Industrial & engineering chemistry research*, Vol. 42, No. 8, 2003, pp. 1603-1618.

[7] Lopez-Echeverry, J.S., S. Reif-Acherman, and E. Araujo-Lopez, "Peng-Robinson equation of state: 40 years through cubics," *Fluid Phase Equilibria*, Vol. 447, No., 2017, pp. 39-71.

[8] Soave, G., "Equilibrium constants from a modified Redlich-Kwong equation of state," *Chemical engineering science*, Vol. 27, No. 6, 1972, pp. 1197-1203.

[9] Peng, D.-Y. and D.B. Robinson, "A new two-constant equation of state," *Industrial & Engineering Chemistry Fundamentals*, Vol. 15, No. 1, 1976, pp. 59-64.

[10] Wang, X. and V. Yang, "Supercritical mixing and combustion of liquid-oxygen/kerosene bi-swirl injectors," *Journal of Propulsion and Power*, Vol. 33, No. 2, 2017, pp. 316-322.

[11] Wang, X., Y. Li, Y. Wang, and V. Yang, "Near-field flame dynamics of liquid oxygen/kerosene bi-swirl injectors at supercritical conditions," *Combustion and Flame*, Vol. 190, No., 2018, pp. 1-11.

[12] Poling, B.E., J.M. Prausnitz, and J.P. O'connell, *The properties of gases and liquids*. Vol. 5. 2001: Mcgraw-hill New York.

[13] Lemmon, E.W., M.L. Huber, and M.O. McLinden, "REFPROP: Reference fluid thermodynamic and transport properties," *NIST standard reference database*, Vol. 23, No. 8.0, 2007.

[14] Péneloux, A., E. Rauzy, and R. Fréze, "A consistent correction for Redlich-Kwong-Soave volumes," *Fluid phase equilibria*, Vol. 8, No. 1, 1982, pp. 7-23.

[15] Cismondi, M. and J. Mollerup, "Development and application of a three-parameter RK–PR equation of state," *Fluid Phase Equilibria*, Vol. 232, No. 1-2, 2005, pp. 74-89.

[16] Ghoderao, P.N.P., V.H. Dalvi, and M. Narayan, "A four-parameter cubic equation of state for pure compounds and mixtures," *Chemical Engineering Science*, Vol. 190, No., 2018, pp. 173-189.

[17] Mathias, P.M. and T.W. Copeman, "Extension of the Peng-Robinson equation of state to complex mixtures: Evaluation of the various forms of the local composition concept," *Fluid Phase Equilibria*, Vol. 13, No., 1983, pp. 91-108.

[18] Stryjek, R. and J. Vera, "PRSV2: a cubic equation of state for accurate vapor—liquid equilibria calculations," *The Canadian Journal of Chemical Engineering*, Vol. 64, No. 5, 1986, pp. 820-826.
[19] Gasem, K.A.M., W. Gao, Z. Pan, and R.L. Robinson, "A modified temperature dependence for the Peng–Robinson equation of state," *Fluid Phase Equilibria*, Vol. 181, No. 1, 2001, pp. 113-125.
[20] Haghtalab, A., M.J. Kamali, S.H. Mazloumi, and P. Mahmoodi, "A new three-parameter cubic equation of state for calculation physical properties and vapor–liquid equilibria," *Fluid Phase Equilibria*, Vol. 293, No. 2, 2010, pp. 209-218.
[21] Joshipura, M., S. Dabke, and N. Subrahmanyam, "Development and comparison of cohesion function relationship for PR equation of state," *Int. J. Chem. Eng. Res*, Vol. 1, No. 2, 2009, pp. 123-134.
[22] Twu, C.H., J.E. Coon, and J.R. Cunningham, "A new generalized alpha function for a cubic equation of state Part 1. Peng-Robinson equation," *Fluid Phase Equilibria*, Vol. 105, No. 1, 1995, pp. 49-59.
[23] Forero G, L.A. and J.A. Velásquez J, "The Patel–Teja and the Peng–Robinson EoSs performance when Soave alpha function is replaced by an exponential function," *Fluid phase equilibria*, Vol. 332, No., 2012, pp. 55-76.
[24] Forero G, L.A. and J.A. Velásquez J, "A modified Patel–Teja cubic equation of state: Part I – Generalized model for gases and hydrocarbons," 342, No., 2013, pp. 8-22.
[25] Kennedy, M.C. and A. O'Hagan, "Bayesian calibration of computer models," *Journal of the Royal Statistical Society: Series B (Statistical Methodology)*, Vol. 63, No. 3, 2001, pp. 425-464.
[26] Tuo, R. and C.J. Wu, "Efficient calibration for imperfect computer models," *The Annals of Statistics*, Vol. 43, No. 6, 2015, pp. 2331-2352.
[27] Plumlee, M., "Bayesian calibration of inexact computer models," *Journal of the American Statistical Association*, Vol. 112, No. 519, 2017, pp. 1274-1285.
[28] Sacks, J., W.J. Welch, T.J. Mitchell, and H.P. Wynn, "Design and analysis of computer experiments," *Statistical Science*, Vol. 4, No. 4, 1989, pp. 409-423.
[29] Bayarri, M.J., J.O. Berger, R. Paulo, J. Sacks, J.A. Cafeo, J. Cavendish, C.-H. Lin, and J. Tu, "A Framework for Validation of Computer Models," *Technometrics*, Vol. 49, No. 2, 2007, pp. 138-154.
[30] Farah, M., P. Birrell, S. Conti, and D.D. Angelis, "Bayesian emulation and calibration of a dynamic epidemic model for A/H1N1 influenza," *Journal of the American Statistical Association*, Vol. 109, No. 508, 2014, pp. 1398-1411.
[31] Higdon, D., M. Kennedy, J.C. Cavendish, J.A. Cafeo, and R.D. Ryne, "Combining field data and computer simulations for calibration and prediction," *SIAM Journal on Scientific Computing*, Vol. 26, No. 2, 2004, pp. 448-466.
[32] Higdon, D., J. Gattiker, B. Williams, and M. Rightley, "Computer model calibration using high-dimensional output," *Journal of the American Statistical Association*, Vol. 103, No. 482, 2008, pp. 570-583.
[33] Gramacy, R.B., D. Bingham, J.P. Holloway, M.J. Grosskopf, C.C. Kuranz, E. Rutter, M. Trantham, and R.P. Drake, "Calibrating a large computer experiment simulating radiative shock hydrodynamics," *The Annals of Applied Statistics*, Vol. 9, No. 3, 2015, pp. 1141-1168.

[34] Patel, N.C. and A.S. Teja, "A new cubic equation of state for fluids and fluid mixtures," *Chemical Engineering Science*, Vol. 37, No. 3, 1982, pp. 463-473.
[35] Ghoderao, P.N.P., V.H. Dalvi, and M. Narayan, "A five-parameter cubic equation of state for pure fluids and mixtures," *Chemical Engineering Science: X*, Vol. 3, No., 2019, pp. 100026.
[36] Caflisch, R.E., "Monte carlo and quasi-monte carlo methods," *Acta numerica*, Vol. 1998, No., 1998, pp. 1-49.
[37] Gramacy, R.B., *Surrogates: Gaussian Process Modeling, Design, and Optimization for the Applied Sciences*. 2020: CRC Press.
[38] Byrd, R.H., P. Lu, J. Nocedal, and C. Zhu, "A limited memory algorithm for bound constrained optimization," *SIAM Journal on scientific computing*, Vol. 16, No. 5, 1995, pp. 1190-1208.
[39] Wang, X., H. Huo, Y. Wang, and V. Yang, "Comprehensive study of cryogenic fluid dynamics of swirl injectors at supercritical conditions," *AIAA Journal*, Vol. 55, No. 9, 2017, pp. 3109-3119.